Analysis of an On-Line Stability Monitoring Approach for DC Microgrid Power Converters

Aram Khodamoradi, *Student Member, IEEE,* Guangyuan Liu, *Student Member, IEEE,*
Paolo Mattavelli, *Fellow, IEEE,* Tommaso Caldognetto, *Member, IEEE,* and Paolo Magnone

***Abstract*—An on-line approach to evaluate and monitor the stability margins of dc microgrid power converters is presented in this paper. The discussed online stability monitoring technique (MT) is based on the Middlebrook's loop-gain measurement technique, adapted to the digitally controlled power converters. In this approach, a perturbation is injected into a specific digital control loop of the converter and after measuring the loop gain, its crossover frequency and phase margin are continuously evaluated and monitored. The complete analytical derivation of the model, as well as detailed design aspects, are reported. In addition, the presence of multiple power converters connected to the same dc bus, all having the stability monitoring unit, is also investigated. An experimental microgrid prototype is implemented and considered to validate the theoretical analysis and simulation results, and to evaluate the effectiveness of the digital implementation of the technique for different control loops. The obtained results confirm the expected performance of the stability monitoring tool in steady-state and transient operating conditions. The proposed method can be extended to generic control loops in power converters operating in dc microgrids.**

***Index Terms*—Digitally-controlled power converters, dc microgrids, frequency estimation, stability monitoring.**

I. Introduction

RECENTLY, there has been an increasing interest towards dc and hybrid dc/ac microgrids. This is mainly because dc microgrids lead to a reduction in distribution losses, are potentially more compatible with home appliances, and allow efficient and effective integration of distributed energy resources (DERs), by taking advantage of power electronic converters features [1]. The typical structure of a dc microgrid with different DERs is displayed in Fig. 1. Besides the electronic-based power conversion stages, a microgrid-level supervisory controller communicating with the DERs converters is often adopted to coordinate the available resources [2].

Many of the resources populating a microgrid change their output terminals behavior during normal operation, as the status of the interfaced resources (e.g., renewable source, storage device) or of the microgrid itself changes. Various kinds of control structures are used to ensure that DERs always keep performing suitably, regardless of the operating conditions. In particular, the power converters involve multiple control loops, such as, the inner output current and voltage, the virtual impedance [3], and the droop loops [4].

The control loops are often designed with reference to a specific operation point, while they show different performances at different points [5], [6]. The fact that the performances of some loops—usually the slowest and the external ones—may be influenced by variables such as the impedance at the point of connection and the control employed in other converters makes the stability of the interaction between the DER converters a critical aspect. A typical example is a power converter behaving as a constant power load (CPL), which is known to present a destabilizing negative incremental impedance at the point of coupling with the dc bus [7], [8]. Another example is the change in the bus impedance when the number of converters connected to the dc bus varies, which leads accordingly, to change in the stability margins of those loops that depend on the bus impedance. Fig. 2 represents this aspect by showing the reduction in the bandwidth of the droop loop of a buck converter, while increasing the number of buck converters connected in parallel to the common dc bus. Of course, this issue can be found exacerbated in practical

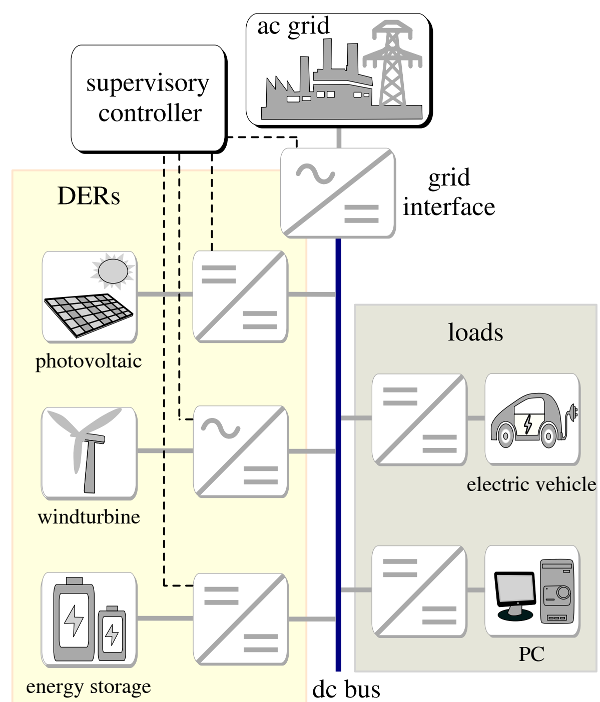

Fig. 1. DC microgrid with distributed energy resources (DERs).

This project has received funding from the University of Padova, PRAT 2015 no. CPDA159190. *(Corresponding author: Aram Khodamoradi)*

The authors are with the Department of Management and Engineering (DTG), University of Padova, Vicenza, 36100, Italy (e-mail: aram.khodamoradi@phd.unipd.it; guangyuan.liu@phd.unipd.it; paolo.mattavelli@unipd.it; tommaso.caldognetto@unipd.it; paolo.magnone@unipd.it).

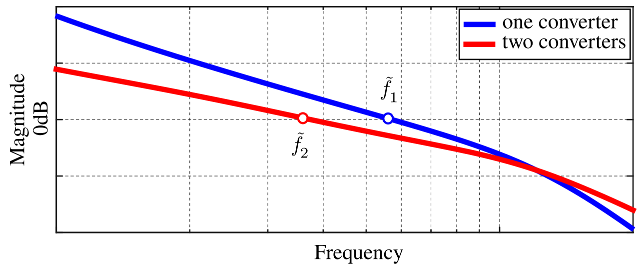

Fig. 2. Transfer function of the droop loop of a buck converter, when having 1 or 2 buck converters are connected to the dc bus (just magnitude is shown here). The two corresponding bandwidths are highlighted in the figure.

applications with a higher number of converters and more diverse topologies.

In the outlined scenario, it is clear that stability measurement and monitoring may be particularly valuable for various purposes. Indeed, reliable stability monitoring techniques can be advantageously exploited to perform crucial tasks in microgrids, such as, condition monitoring for reliability purposes, on-line tuning of power converters controllers, and adaptive control. A significant example of the latter case can be found in shipboard dc power distribution systems, where the behavior seen by a converter from its load and source sides can tremendously change along the course of a mission; this rises stability concerns about the interactions among the subsystems. In this context, continuous, online estimates of the stability-margins can be effectively exploited to tune the converters controllers, thus ensuring a reliable operation [9].

Different approaches to measure the loop gains and evaluate the system stability margins under various conditions are reported in the literature. In [10], [11], some methods to measure the frequency response of a converter's loop gain are proposed. In [12], [13] auto-tuning is achieved on the basis of the online assessment of the loop gain frequency response. Authors in [7] and [14] propose an approach based on voltage or current perturbations to find the open-loop transfer functions for stability analysis, which is based on the well-known impedance-based stability criterion [8]. In [15] control-to-output frequency response is calculated using a cross-correlation approach. In this method, a pseudo-random binary sequence (PRBS) is added to the duty cycle of a converter and, by assuming the converter as a linear time-invariant (LTI) system, the output voltage or current is measured. Then, the cross-correlation between the input and the output is found, and the impulse response of the system is calculated under the assumption that the PRBS signal is a good approximation of white-noise. Finally, by performing a discrete Fourier transform, the frequency response of the system is found.

Recently, many system identification approaches based on the frequency response have been proposed for the stability analysis of converters controllers [16]–[19]. These approaches typically consider the system of interest as a black-box model [16], [17] or a grey-box model [18], [19] and, when the error between the real system behavior and the corresponding model behavior is minimized, an accurate model is deemed to have been obtained. The black-box model, also known as non-parametric system identification technique, features a low complexity level and does not require prior knowledge of the model to be estimated. The drawbacks of this method are long sequences of data to be acquired, slow response times, and inability of dealing with rapid system variations. On the other hand, the grey-box method, also known as parametric system identification technique, has a higher level of complexity, because the structure of the targeted model must be defined in advance. In particular, it is appropriate for switched-mode power supplies (SMPS), due to the initial assumption of the dc-dc converter to behave as a second order system. However, all the system identification methods are applied when the system is operating in steady-state; consequently, a new model of the system must be identified in case of any variations in the steady-state operating condition.

Middlebrook's analog injection technique [20] is the basis of some other studies. It is the case of [21], which reports the application of the online measurement of crossover frequency and phase margin in digitally controlled SMPSs during normal operating conditions. A digital small-signal perturbation is added in series with the converters control loop and stability monitoring is performed on the basis of loop gain measurements around the unity-gain frequency (i.e., crossover frequency). This method is verified referring to the voltage control loop of low-voltage buck and boost converters, showing its ability to continuously estimate the crossover frequency and the phase margin without opening the feedback loop, and even in presence of load transients.

Reference [21] targets stability monitoring for specific kinds of dc-dc converters, featuring low voltage levels, high switching frequencies, and FPGA-based controllers. On the basis of the same concept, this paper proposes a stability monitoring technique for the parallel operation of multiple converters, which becomes, in recent years, an aspect of interest in microgrid applications. The DERs converters within a microgrid feature completely different characteristics with respect to those considered in [21]. Therefore, an alternative signal processing, with low implementation complexity, is proposed in this paper. In addition, the complete analytical model of the stability monitoring unit, is derived and addressed in this paper. The proposed monitoring technique is robust to noise and the perturbations coming from other converters connected in parallel to the common dc bus. Moreover, since it has a low implementation complexity and fast response time, it can be useful for future investigations on adaptive tuning techniques for converters in dc microgrids.

The preliminary results of this study are partially presented in [22], while this paper provides the comprehensive description of the technique, and explains the brought improvements, by reporting *a*) the complete discussion of the theoretical analysis and detailed design aspects, *b*) the experimental validation of the proposed method implemented in a multi-converter prototype, *c*) the situation of having multiple converters simultaneously performing the stability monitoring. The last point is a typical issue in microgrids when two or more converters inject a small-signal perturbation at the same time, with frequencies that can be close to each other. In general, the effects of different perturbation signals can get combined, leading to an error in the process of tracking the unity loop-gain frequency. To address this issue, a prioritization-based technique is considered, such that, just one converter is allowed to inject the small-signal perturbation at a certain time. For more critical cases, where simultaneous monitoring is required in several converters, it is shown that a small modification in the way the unity-gain frequency is extracted allows to minimize the error resulted from the combination of the perturbation signals.

The remainder of the paper is organized as follows. Sec. II briefly explains the basics of online monitoring technique referring to a generic converter control loop. Sec. III presents the proposed approach and discusses the related design aspects. Sec. IV discusses the situation in which two or more converters need to monitor the stability margins simultaneously. Sec. V describes the application of the proposed monitoring scheme to power converters implementing the droop control. Sec. VI presents the prototype implemented to verify the proposed approach and discusses the obtained experimental results. Sec. VII reports the conclusions of this study.

II. Concept Description

Middlebrook's injection technique [20] is well known and widely used to measure the frequency response of an analog system control loop without interrupting the feedback path. The technique consists in injecting a small-signal perturbation at a certain frequency into the considered control loop in order to stimulate and acquire the system behavior at that frequency. The stability monitoring technique presented herein is based on the same concept, but applied to digitally-controlled converters. Digital control platforms are usually preferable over the analog counterpart in several environments, including the microgrid one [23]. This is because the digital approach features programmability, reduced need to external passive components, high integration capability, and the intrinsic ability to implement complex functions, which is a crucial aspect for stability monitoring, auto-tuning, and other similar tasks [24].

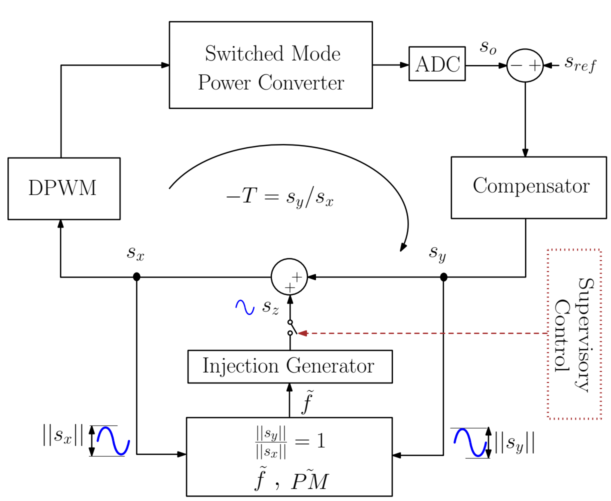

Fig. 3. Stability monitoring of a generic control loop of a digitally-controlled SMPS.

Fig. 3 schematically represents the proposed monitoring technique applied to a generic control loop of a digitally controlled power converter. Regardless of the specific loop (e.g., current, voltage, or power control loop), the main components of a digital controller implementation are reported in Fig. 3, including, in particular, an analog-to-digital converter (ADC), a discrete-time compensator, and a digital pulse width modulator (DPWM). The perturbation signal s_z, with frequency $\tilde{f}$, can be injected ideally at any point of the digital control loop. Notably, the digital implementation is free from any loading effect, which is an advantage over the analog case.

By referring to Fig. 3, the system loop gain evaluated at $\tilde{f}$ is:

$$T(s)|_{s=j2\pi\tilde{f}} = -\left.\frac{s_y(s)}{s_x(s)}\right|_{s=j2\pi\tilde{f}} = -\frac{s_y(j\,2\pi\tilde{f})}{s_x(j\,2\pi\tilde{f})} \qquad (1)$$

where s_x and s_y are the signals after and before, respectively, the perturbation injection point. By definition, the crossover frequency f_c of the control loop corresponds to the frequency $\tilde{f}$ of the perturbation signal at which the open-loop transfer function shows unity gain; that is, if:

$$|T(j\,2\pi\tilde{f})| = 1 \qquad (2)$$

then:

$$f_c = \tilde{f} \qquad (3)$$

and:

$$\begin{aligned} PM = \tilde{PM} &= 180^\circ + \angle T(j\,2\pi\tilde{f}) \\ &= \angle s_y(j\,2\pi\tilde{f}) - \angle s_x(j\,2\pi\tilde{f}) \end{aligned} \qquad (4)$$

where PM and $\tilde{PM}$ indicate, respectively, the true and the estimated values of the phase margin. It is worth to remark that this approach is valid for systems with a loop gain higher than unity (i.e., $|T(j2\pi f)| > 1$) for some frequencies, which is almost always the case; otherwise, the stability margin cannot be assessed in this way, because there are no zero-crossings.

On the basis of this, the operation principle of the proposed crossover frequency and phase-margin estimation technique is to adjust the frequency $\tilde{f}$ of the injected perturbation s_z so as to have the amplitude difference between the two signals s_x and s_y converging to zero. In such an operating point (i.e., $|s_y| - |s_x| = 0$), (2)-(4) hold, therefore, the frequency $\tilde{f}$ and the phase shift between s_x and s_y are monitored and referred to as the crossover frequency and the phase margin of the considered control loop, respectively.

It is worth remarking that the small-signal perturbation can be injected in any control loop of the power converter, as far as that loop is stable—even with low stability margins. The information obtained by the monitoring process may eventually be exploited to perform provisions that keep the loop under investigation far from instability (e.g., by auto-tuning the associated regulators).

III. Proposed Estimation Technique

A. Proposed phase margin and crossover frequency estimator

Fig. 4 displays the technique that is here proposed for the estimation of the crossover frequency and phase margin of a control loop. First of all, a sine wave generator is used to produce a small-signal perturbation s_z of amplitude $|s_z|$ and frequency $\tilde{f}$. The signal s_z is injected into the control loop, resulting in a perturbation at the same frequency in the signals s_x and s_y. Similarly to common and well-known projections used in signal processing (e.g., to find the Fourier series of a signal), the two signals s_x and s_y are multiplied by sine and cosine terms at the estimated crossover frequency $\tilde{f}$. By doing so, it is possible to derive the signal projections into a common reference frame defined by the in-phase (i.e., sin) and the quadrature (i.e., cos) components of the injected perturbation s_z. The obtained projections can be represented in any two-dimensional reference plain, like, for example, the complex plane. Herein, the components of s_x and s_y at frequency $\tilde{f}$ are represented by a real and an imaginary part as $s_x^R + js_x^I$ and $s_y^R + js_y^I$.

To describe this process analytically, let us assume a linear and time-invariant (LTI) system. The effect of the perturbation s_z in a specific loop, can be represented as a sinusoidal signal at $\tilde{f}$, with a certain magnitude and phase:

$$s_x = |s_x|\cos(2\pi\tilde{f}t+\angle s_x), \quad s_y = |s_y|\cos(2\pi\tilde{f}t+\angle s_y) \quad (5)$$

By projecting s_x along the real and the imaginary axes we get:

$$s_x(t)\sin(2\pi\tilde{f}t) = -\frac{|s_x|}{2}\sin(\angle s_x) + \frac{|s_x|}{2}\sin(4\pi\tilde{f}t + \angle s_x) \quad (6)$$

$$s_x(t)\cos(2\pi\tilde{f}t) = \frac{|s_x|}{2}\cos(\angle s_x) + \frac{|s_x|}{2}\cos(4\pi\tilde{f}t + \angle s_x) \quad (7)$$

The same holds for s_y. The dc values of the results in (6) and (7) are, respectively, the imaginary and the real components of the signal s_x at $\tilde{f}$ (the same applies for s_y). In Fig. 4 the dc values are estimated by low-pass filters (LPFs) with transfer function $G_{LPF}(s)$.

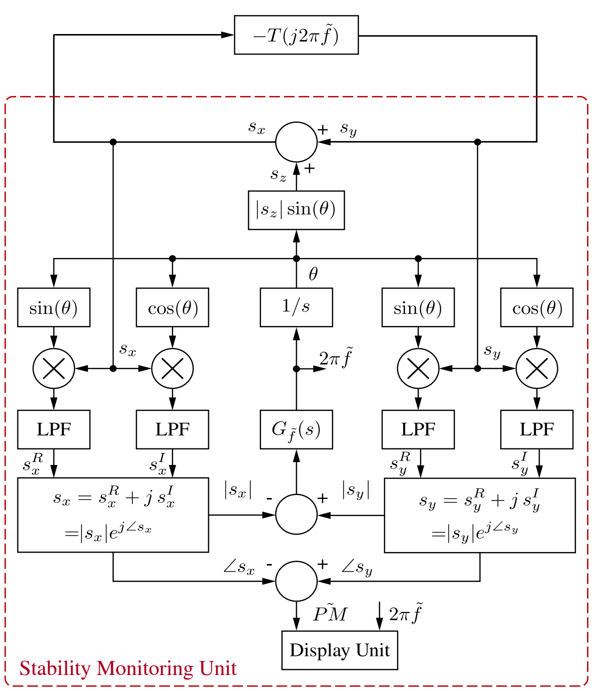

Fig. 4. Scheme of the proposed online stability monitoring technique.

Equations (6) and (7) after low-pass filtering can be written as:

$$LPF\left(s_x(t)\sin(2\pi\tilde{f}t)\right) = -\frac{|s_x|}{2}\sin(\angle s_x) + G_{LPF}(j4\pi\tilde{f}).\frac{|s_x|}{2}\sin(4\pi\tilde{f}t + \angle s_x) \quad (8)$$

$$LPF\left(s_x(t)\cos(2\pi\tilde{f}t)\right) = \frac{|s_x|}{2}\cos(\angle s_x) + G_{LPF}(j4\pi\tilde{f}).\frac{|s_x|}{2}\cos(4\pi\tilde{f}t + \angle s_x) \quad (9)$$

If the cut-off frequency of the LPFs f_{lpf} is significantly smaller than $\tilde{f}$, the gain of the LPF at twice the estimated crossover frequency, namely, $|G_{LPF}(j4\pi\tilde{f})|$, is small, and the high frequency components in (8) and (9) can be neglected. This means that (8) and (9) can precisely estimate $s_x^I = -\frac{|s_x|}{2}\sin(\angle s_x)$ and $s_x^R = \frac{|s_x|}{2}\cos(\angle s_x)$, respectively. Then, the obtained imaginary and real components can be used to evaluate the magnitude and phase of s_x and s_y, by using the arc tangent and square-root functions. Therefore, based on estimating the quantities $|s_x|$, $|s_y|$, $\angle s_x$, and $\angle s_y$, an accurate estimation of the phase margin and crossover frequency can be reached. The particular choice of f_{lpf} has an effect on the estimated stability margins, which is shown in Sec. VI by means of numerical data. In general terms, according to (8) and (9), f_{lpf} should be significantly smaller than the crossover frequency, but it should not be so small to affect the design of the frequency loop regulator $G_{\tilde{f}}$, as explained later in this section.

The difference in amplitudes $|s_y| - |s_x|$ is processed by the frequency regulator $G_{\tilde{f}}$ in Fig. 4, whose output is the frequency of the perturbation signal. By including an integral part in $G_{\tilde{f}}$, the difference in the amplitudes converges to zero (i.e., $|s_x| = |s_y|$), because of the unity loop gain condition discussed in Sec. II. At this point, the frequency of the perturbation signal is equal to the crossover frequency of the considered loop, while the phase margin is calculated as the phase shift between $s_x(j2\pi\tilde{f})$ and $s_y(j2\pi\tilde{f})$.

Finally, it is worth remarking that the signal processing of the proposed scheme shown in Fig. 4 can be also implemented in other ways, such as the one based on band-pass filters (BPF) adopted in [21]. However, this choice would require a BPF implementation that automatically adapts its center frequency, bandwidth, and Q-factor according to the loop under investigation, resulting in an increase in the response time and computational burden, which may be critical.

B. Design of the frequency loop regulator $G_{\tilde{f}}$

The regulator $G_{\tilde{f}}$ performs the regulation of the perturbation frequency $\tilde{f}$ on the basis of the measured difference in the amplitude of the two signals s_x and s_y (i.e., $|s_y| - |s_x|$). A model of this frequency control loop is therefore required for the design of $G_{\tilde{f}}$. However, due to system non-linearities, a general and rigorous analytical procedure for modeling this loop is not trivial and would require dedicated investigations. Instead, in the following, two simplifying assumptions are introduced, which allow to approximate the frequency loop model and design the regulator $G_{\tilde{f}}$.

Assumption 1: The dynamics of the frequency control loop is mostly determined by the LPFs used in the MT described in Fig. 4. As explained in Sec. III-A, the cut-off frequency of the LPFs f_{lpf} must be significantly smaller than $\tilde{f}$ to have a precise amplitude estimation. Based on this condition and the fact that the rest of the MT process is much faster than the low-pass filtering part, assumption 1 represents a reasonable approximation of the system dynamics. Under assumption 1, the open-loop transfer function from the injection frequency $\tilde{f}$ to the amplitude difference $|s_y| - |s_x|$ can be approximated as:

$$T_{\tilde{f}}(s) = \frac{[|s_y| - |s_x|]\,(s)}{\tilde{f}(s)} \simeq K_{\tilde{f}} \cdot G_{LPF}(s) \tag{10}$$

where $K_{\tilde{f}}$ is the static gain:

$$K_{\tilde{f}} = \left.\frac{\partial\left[|s_y(j2\pi f)| - |s_x(j2\pi f)|\right]}{\partial f}\right|_{f=\tilde{f}} \tag{11}$$

By referring to Fig 4, it is possible to notice that:

$$s_x(j2\pi f) = \frac{1}{1+T(j2\pi f)} s_z(j2\pi f) \tag{12}$$

$$s_y(j2\pi f) = -\frac{T(j2\pi f)}{1+T(j2\pi f)} s_z(j2\pi f) \tag{13}$$

Therefore, substituting (12) and (13) in (11), and assuming s_z generated with constant amplitude $|s_z|$, the value of $K_{\tilde{f}}$ can be expressed as:

$$\begin{aligned} K_{\tilde{f}} &= \left.\frac{\partial\left[|s_y(j2\pi f)| - |s_x(j2\pi f)|\right]}{\partial f}\right|_{f=\tilde{f}} \\ &= |s_z|\left.\frac{\partial}{\partial f}\left(\frac{|T(j2\pi f)|-1}{|1+T(j2\pi f)|}\right)\right|_{f=\tilde{f}} \end{aligned} \tag{14}$$

According to the basic differentiation identities for the derivative of a generic rational expression, and based on the fact that $|T(j2\pi\tilde{f})|\Big|_{f=\tilde{f}} \simeq 1$, (14) can be written as follows:

$$\begin{aligned} K_{\tilde{f}} &= |s_z|\left.\frac{|1+T(j2\pi f)|\cdot\frac{\partial|T(j2\pi f)|}{\partial f}}{|1+T(j2\pi f)|^2}\right|_{f=\tilde{f}} \\ &- |s_z|\left.\frac{(|T(j2\pi f)|-1)\cdot\frac{\partial|1+T(j2\pi f)|}{\partial f}}{|1+T(j2\pi f)|^2}\right|_{f=\tilde{f}} \\ &= |s_z|\left.\frac{\frac{\partial|T(j2\pi f)|}{\partial f}}{|1+T(j2\pi f)|}\right|_{f=\tilde{f}} \end{aligned} \tag{15}$$

which, based on Euler's formula, can be simplified as follows (again $|T(j2\pi\tilde{f})|\Big|_{f=\tilde{f}} \simeq 1$):

$$K_{\tilde{f}} = |s_z|\left.\frac{\frac{\partial|T(j2\pi f)|}{\partial f}}{\sqrt{2}\sqrt{1+\cos(\angle T(j2\pi f))}}\right|_{f=\tilde{f}} \tag{16}$$

In the case that the loop gain T is not known a priori, suitable approximation or estimations around the crossover frequency may be considered, like the assumption introduced below.

Assumption 2: The slope of $|T(j2\pi f)|$ and the phase of T around the crossover frequency (i.e., $\left.\frac{\partial|T(j2\pi f)|}{\partial f}\right|_{f=\tilde{f}}$, and $\angle T(j2\pi f)|_{f=\tilde{f}}$) are -20 $\mathrm{dB/decade}$ and 90 deg, respectively. These two estimations of the system behavior are considered to give a reasonable approximation of a second order stable system and do not have general validity. For example, if the approximated phase of T around the crossover frequency is assumed to be 60 deg instead 90 deg, based on (16), a difference of about 10% in the estimation of $K_{\tilde{f}}$ can be expected.

Different choices are possible to implement $G_{\tilde{f}}$, herein a pure integrator is considered and designed on the basis of the desired bandwidth of the frequency control loop $f_{c,\tilde{f}}$:

$$G_{\tilde{f}}(s) = \frac{2\pi f_{c,\tilde{f}}}{K_{\tilde{f}}}.\frac{1}{s} \tag{17}$$

giving a theoretic value of phase margin equal to $\pi/2 + \mathrm{phase}[\text{LPF}(j2\pi f_{c,\tilde{f}})]$, which results in generous margins in case $f_{c,\tilde{f}}$ is significantly lower than the cut-off frequency f_{lpf} of the low-pass filters. This design is actually a conservative option. Of course, if required, $f_{c,\tilde{f}}$ can be further increased; in this case, the phase margin of the MT loop should be evaluated and taken into account.

Finally, it is worth remarking that the response time of the proposed MT depends on the regulator $G_{\tilde{f}}$, which, in turn, depends on the actual system parameters (i.e., T). However, the stability of the MT can be ensured by choosing sufficiently wide stability margins for the frequency control loop. For validation purposes, the considered model has been evaluated in simulation considering a buck converter with the parameters listed in Sec. VI. A unitary step change has been applied to the injected perturbation frequency $\tilde{f}$ and the open loop step response of the amplitude difference $|s_y| - |s_x|$ has been observed. In these conditions, the variation in the value of $|s_y|-|s_x|$ presents about 5% error with respect to the estimated static gain $K_{\tilde{f}}$. Also, the observed rise-time matches, with a similar precision, the set value of bandwidth $f_{c,\tilde{f}}$. In the light of this the design of the regulators used in the experimental setup in Sec. VI is performed.

IV. MULTIPLE CONVERTER SCENARIO

When multiple, independent, paralleled converters with similar crossover frequencies perform stability monitoring at the same time, the injected perturbation signals combine and the accuracy of the unity-gain criterion (2) and (3) may reduce. Different solutions have been proposed to cope with similar issues [25], [26]. The following paragraphs discuss this aspect, presenting a general approach, based on supervisory control, and a practical method for handling the issue in some cases of interest.

A. Non-simultaneous monitoring

In many practical applications, *simultaneous* stability monitoring is not strictly required. In these cases, different time slots for perturbation injection can be assigned to the converters and the stability monitoring in the converters activated sequentially without overlaps. The activation scheme can be defined, for example, by time division multiplexing algorithms, inspired by the telecommunication engineering solutions used in multi-antenna systems [27]. Here a supervisory control is adopted, which can be implemented in many ways, such as, the token ring technology [28]. In this way, a supervisory unit (as displayed in Fig. 3) issues an activation command to the converters for enabling the monitoring unit. The activation command is sequentially assigned to the converters according to predetermined criteria. Clearly, the rate at which the token is reassigned determines the time of convergence, which is an important aspect when the information provided by the monitoring tool is employed for controllers tuning.

B. Simultaneous monitoring

In less common but still realistic scenarios, the simultaneous stability monitoring of multiple converters is required. A relevant example can be the connection of additional converters to a distribution bus, which changes the bus impedance and so the stability margins of the other converters that may be initially connected. In this case, each converter must monitor its stability margins on-line, to make sure that the applied changes do not create additional instability issues. By referring to the proposed scheme discussed in the previous section, the simultaneous monitoring of stability margins at more than one converter is addressed below. For simplicity, in this part of the analysis a two-converter system is referred to; but the same discussion can be made also for systems with more converters. When having two converters injecting sinusoidal perturbation signals on the dc bus, we firstly observe that s_y in (5) can be modified in the following form (the same holds for s_x):

$$s_y = |s_{y1}|\cos(2\pi\tilde{f}_1 t+\angle s_{y1})+|s_{y2}|\cos(2\pi\tilde{f}_2 t+\angle s_{y2}) \quad (18)$$

where subscript 1 refers to the first converter and subscript 2 refers to the second one. Based on the projection technique detailed in Fig. 4, the translation of each signal s_x, s_y along the sine term (or cosine term, similarly) of the estimated crossover frequency $\tilde{f}$ of each converter can be formulated. At converter #1, by exploiting the well-known trigonometric identities, it yields:

$$\begin{aligned} s_y(t)\sin(2\pi\tilde{f}_1 t) &= \{|s_{y1}|\cos(2\pi\tilde{f}_1 t+\angle s_{y1}) \\ &\quad + |s_{y2}|\cos(2\pi\tilde{f}_2 t+\angle s_{y2})\}\sin(2\pi\tilde{f}_1 t) \\ &= \frac{|s_{y1}|}{2}\{\sin(4\pi\tilde{f}_1 t+\angle s_{y1})-\sin(\angle s_{y1})\} \\ &\quad + \frac{|s_{y2}|}{2}\{\sin(2\pi(\tilde{f}_1+\tilde{f}_2)t+\angle s_{y2}) \\ &\quad - \sin\left(2\pi(\tilde{f}_2-\tilde{f}_1)t+\angle s_{y2}\right)\} \end{aligned} \quad (19)$$

As discussed in Sec. III-A, the cut-off frequency of the low-pass filters is significantly smaller than the crossover frequency; thus, the effect of the sinusoidal term at frequency $\tilde{f}_2-\tilde{f}_1$ is negligible. As far as the two frequencies $\tilde{f}_1$ and $\tilde{f}_2$ are significantly different, (19) still approximates the dc term $s_y^I = -\frac{|s_{y1}|}{2}\sin(\angle s_{y1})$ with a good precision (a similar consideration holds for s_y^R). This means that the proposed scheme allows multiple converters to monitor their stability margins simultaneously and independently. Because, in each converter the effect of other converters with different perturbation frequencies is discarded, thanks to the orthogonality property.

However, it might be possible that at least two converters with similar crossover frequencies need to perform the monitoring simultaneously. In this case, (19) after low-pass filtering can be written as:

$$\begin{aligned} s_y(t)\sin(2\pi\tilde{f}_1 t) &= -\frac{|s_{y1}|}{2}\sin(\angle s_{y1}) - \\ G_{LPF}(j2\pi(\tilde{f}_2-\tilde{f}_1))&\frac{|s_{y2}|}{2}\sin\left(2\pi(\tilde{f}_2-\tilde{f}_1)t+\angle s_{y2}\right) \end{aligned} \quad (20)$$

in which $\tilde{f}_1 \simeq \tilde{f}_2$. The sinusoidal term at frequency $\tilde{f}_2-\tilde{f}_1$ makes the extraction of the dc term s_y^I more difficult with respect to the case of single perturbation and leads, accordingly, to an error in the amplitude estimation. Of course, this issue worsens as the number of such converters increases.

The solution proposed herein is to modify the design of the LPFs used; in particular, by significantly decreasing the cut-off frequency of the LPF, or by changing its structure (e.g., increase the filter order). So doing, the effect of the term $\tilde{f}_2-\tilde{f}_1$ can be better reduced, thanks to the higher filtering properties, achieving a better amplitude estimation. Clearly, this improvement comes at the price of a correspondingly slower response time of the monitoring process, that is a trade-off between accuracy and speed to be taken depending on the application.

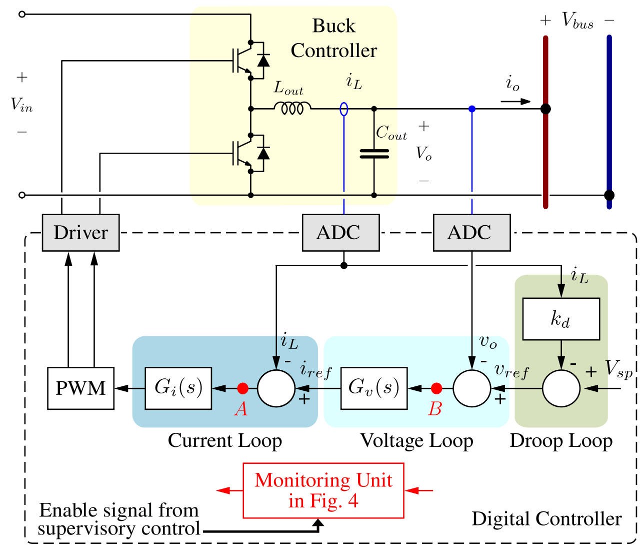

Fig. 5. Droop-controlled converter equipped with the stability monitoring unit. For monitoring the stability margins of the current loop the monitoring unit is inserted at point A, with the other loops open. As for the voltage and droop loops, the monitoring unit is inserted at point B, having the droop loop open and closed, respectively. The activation status of the stability monitoring unit is decided by the enable signal from the supervisory control.

V. APPLICATION TO DROOP-CONTROLLED CONVERTERS

The droop control is proposed in the literature to address various needs of dc microgrids, such as, bus voltage regulation, power sharing among sources, management of storage units,

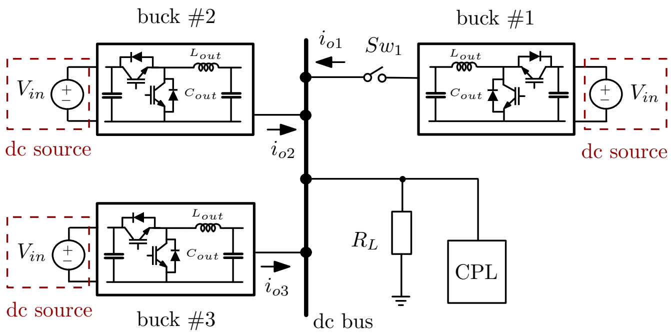

Fig. 6. Considered dc microgrid prototype. Each of the droop-controlled buck converters implements the control structure displayed in Fig. 5.

and islanded operation [4], [29]. The droop control scheme considered in this paper is shown in Fig. 5. The inductor current i_L is sensed and used in the droop loop to produce the reference output voltage v_{ref} needed for the inner voltage loop:

$$v_{ref} = V_{sp} - k_d \cdot i_L \tag{21}$$

where V_{sp} is the dc bus voltage set-point and k_d is the droop coefficient. This allows bus voltage regulation and an automatic sharing of the power needs of the microgrid. Notably, due to the buck converters topology, the inductor current and the output current are equal in the steady-state conditions, thus no additional sensing is required.

The application of the proposed monitoring tool to the droop-controlled converters operating in dc microgrids is investigated in this work. Specifically, three different loops are considered: the inner inductor current control loop, the output voltage control loop, and the droop control loop, as shown in Fig. 5. When the monitoring unit is inserted at point A, while the other loops are open, the stability margins of the current loop is monitored. By inserting the monitoring unit at point B, while the droop loop is open, the stability margins of the voltage loop is monitored. The perturbation is inserted in point B for the droop loop too, but having all the other loops closed. The regulators parameters for the current and voltage loops can be designed based on standard procedures, as discussed, for example, in [24].

VI. SIMULATION AND EXPERIMENTAL RESULTS

The prototype considered in this paper is shown in Fig. 6, which emulates an islanded dc microgrid. It consists of three droop-controlled buck converters, a converter behaving as CPL, and a resistive load, all connected to a common dc bus. The three buck converters implement the same hardware and the same control structure which is shown in Fig. 5. Table II lists the regulators parameters, notably, converters #1 and #2 use the same parameters values, which are different from those of converter #3. In the following, the switch Sw_1 is always closed, apart from the case concerning the transient behavior of the system. All the relevant parameters of the experimental setup are reported in Table I.

The technique is firstly developed and analyzed by simulation models in Matlab/Simulink. Then, the designed regulators, together with the proposed monitoring technique, have been

TABLE I
PARAMETERS OF THE SETUP SHOWN IN FIG. 6

Parameter	Symbol	Value
Input voltage	V_{in}	380 V
Nominal bus voltage	V_{bus}	200 V
Nominal power	P^{nom}	3 kW
Output side inductance	L_{out}	1.6 mH
Output side capacitance	C_{out}	110 µF
Switching frequency	f_{sw}	12.5 kHz
Load Resistance	R_L	150 Ω
Rated power of the CPL	P_{CPL}	3 kW

TABLE II
REGULATORS PARAMETERS OF THE CONVERTERS IN FIG. 6

Parameter	Symbol	Value
current loop		
Current regulator of all converters	G_i	$0.02 + 74.89/s$
voltage loop		
Voltage regulator of buck #1, #2	$G_v^{\#1,\#2}(s)$	$0.21 + 544/s$
Voltage regulator of buck #3	$G_v^{\#3}(s)$	$0.1 + 272/s$
droop loop		
Voltage set point	V_{sp}	200 V
Droop coefficient	k_d	1.33 V/A

deployed in the digital controller of the prototype, which is based on a Texas Instrument DSP (TMS320F2810) operating at 150 MHz. To this end, the analog-to-digital converter (ADC) of the DSP samples the output voltage and the inductor current once per switching period (i.e., $f_{sampling} = f_{sw} = 12.5\,\text{kHz}$), with a resolution of 12 bit. In the DSP code, the MT in Fig. 4 is performed first; then, the converters controllers are implemented to obtain the new value of the duty cycle; finally, the drive signals are generated by means of the PWM modules of the DSP. The measured total execution time of the implemented MT is $14.8\,\mu\text{s}$, without any specific code optimization.

In order to evaluate the performance of the proposed MT, the stability margin values monitored in the experimental model are compared to those represented by the actual transfer function of the experimental setup, which is acquired by means of the Sweep Frequency Response Analysis (SFRA) tool [30]. The analytical and the actual transfer functions of different control loops have been evaluated and compared. However, herein, due to space constraints, just the transfer functions related to the droop loop of converter #2 are reported in Fig. 7. Of course, the loop under study is affected by the other converters in the prototype, and this effect is included in the displayed transfer functions. The close matching between the transfer functions found analytically and those of the experimental setup measured by the SFRA tool, proves the correctness of the adopted models.

In the following, the experimental results obtained by applying the stability monitoring tool to three different control loops are reported and discussed. In particular, the MT is applied to the single converter's inner current and voltage loops and

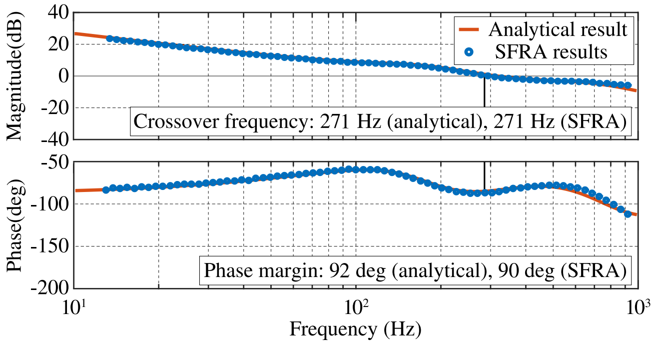

Fig. 7. Droop loop transfer function of converter #2 in Fig. 6: analytical versus experimental data. The effect of the other converters on the considered loop is taken into account. All the relevant parameters are reported in Table II and Table I.

TABLE III
EXPECTED VALUES OF THE STABILITY MARGINS, AND THE MT RESULTS

	crossover frequency	phase margin
current loop of a single converter		
Expected from transfer function (analytical model)	1000 Hz	60 deg
Expected from transfer function (SFRA results)	1000 Hz	58 deg
Monitored online (simulation)	1003 Hz	58 deg
Monitored online (experimental)	1014 Hz	56 deg
voltage loop of converter #2		
Expected from transfer function (analytical model)	460 Hz	40 deg
Expected from transfer function (SFRA results)	460 Hz	41 deg
Monitored online (simulation)	458 Hz	39 deg
Monitored online (experimental)	450 Hz	38 deg
droop loop of converter #2		
Expected from transfer function (analytical model)	271 Hz	92 deg
Expected from transfer function (SFRA results)	271 Hz	90 deg
Monitored online (simulation)	272 Hz	89 deg
Monitored online (experimental)	271 Hz	91 deg

to the droop loop of each of the three droop-controlled buck converters. As we are dealing with a multi-converter setup, the supervisory control described in Sec. IV is adopted to activate the monitoring units of different converters sequentially and without overlaps.

The effect of the small-signal perturbation on the output signals is derived analytically in the Appendix. The amplitude of the sinusoidal perturbation is set in such a way that, after injecting the perturbation in any of the loops, the output current and voltage ripples due to perturbation injection are reasonably low in steady-state (in the case herein considered, less than two percent of the rated values), but still larger than the quantization and noise levels.

A. MT applied to the inner current and voltage loops

In this subsection, the MT is applied at point A in Fig. 5 (with the voltage and droop loops open) and at point B (with the droop loop open), to monitor the stability margins of the current and the voltage loops of a single buck converter, respectively.

The results obtained by the simulation models replicating the experimental setup are shown in Table III. The MT results are close to those expected from the analytical models. Detailed simulation results of the MT applied to the current loop are shown in Fig. 8. The resulting perturbation frequency of the two signals s_y and s_x is equal to the crossover frequency and the phase difference is equal to the phase margin, as expected from (2) and (4), respectively. The same good matching has been achieved considering the voltage loop (the results are not reported herein due to space constraints).

The experimental results of the monitoring tool applied to the current and voltage loops are shown in Fig. 9 and Fig. 10, respectively. As reported in Table III, on the basis of the transfer functions of the experimental setup found by the SFRA tool, the expected values of the crossover frequency and phase margin for the current loop are 1000 Hz and 58 deg, respectively. The estimates from the MT shown in Fig. 9 are 1014 Hz, for the crossover frequency, and 56 deg, for the phase margin. As for the voltage loop, the expected crossover frequency and phase margin are 460 Hz and 41 deg, respectively; the estimates from the MT correspond to 450 Hz

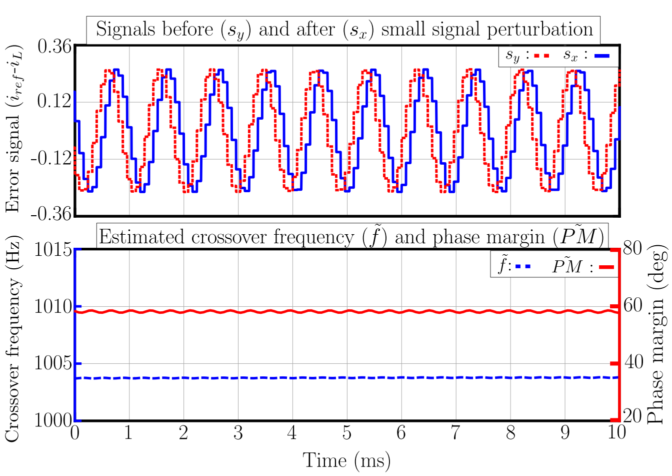

Fig. 8. Simulation results of the current loop stability monitoring. Parameters listed in Table I and Table II.

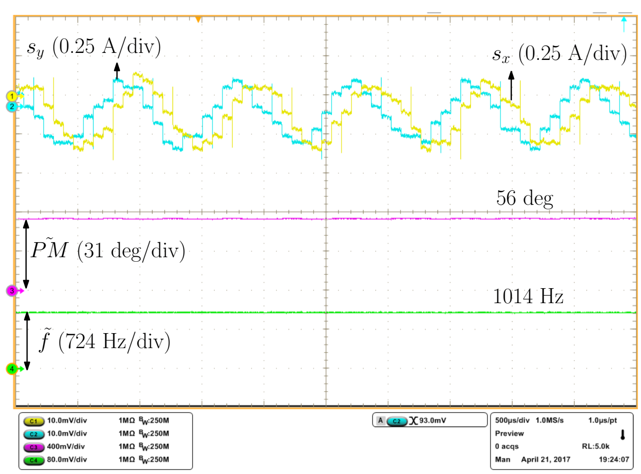

Fig. 9. Experimental results of the current loop stability monitoring. Signals s_y and s_x (before and after injecting the small-signal perturbation), crossover frequency $\tilde{f}$, and phase margin $\tilde{PM}$. Time scale: 0.5 ms/div.

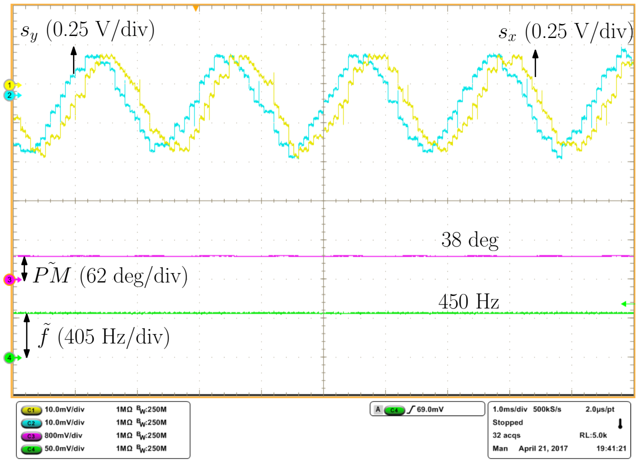

Fig. 10. Experimental results of the voltage loop stability monitoring. Signals s_y and s_x, crossover frequency $\tilde{f}$, and phase margin $\tilde{PM}$. Time scale: 1 ms/div.

and 38 deg, as reported in Fig. 10. The obtained results are consistent and show that the MT performs well in steady-state conditions, for both the current and voltage loops. From Fig. 9 and Fig. 10 it is also possible to notice that the amplitudes of the digital signals before and after injecting a small-signal perturbation (i.e., s_y, s_x) tend to be equal in steady-state, which corresponds to the condition stated in (2).

Fig. 11 shows the ripples in the steady-state waveforms of the input and output voltages and the inductor current in presence of the small-signal perturbations injected for monitoring the current (Fig. 11.a) and voltage (Fig. 11.b) loops. In addition, the duty-cycle fluctuations for the case of current loop is also displayed in Fig. 11.a. It is possible to notice that the ripple stays within a reasonable range. In the case of the current loop, less than 0.5 V and 0.2 A ripple in the output voltage and the inductor current, respectively; in the case of the voltage loop, the measured ripples are slightly larger than the current loop case, but still low enough to not significantly affect the normal operation of the system.

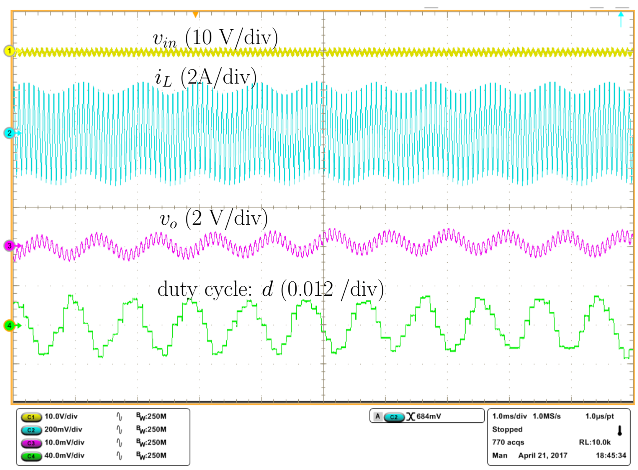

(a) Small signal perturbation in the current loop

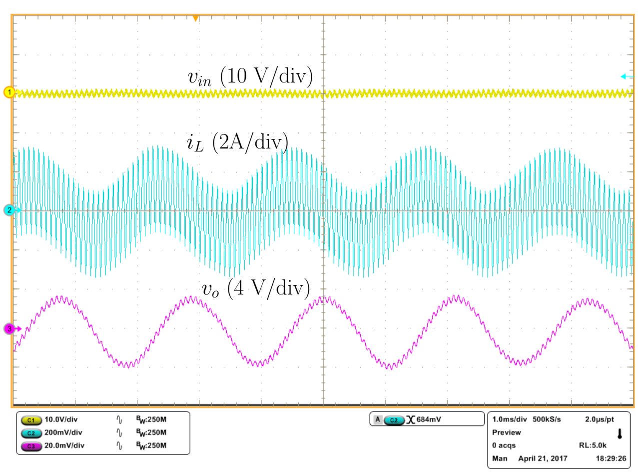

(b) Small signal perturbation in the voltage loop

Fig. 11. Ripples in the steady-state waveforms (input voltage v_{in}, output voltage v_o, inductor current i_L), in presence of small-signal perturbations. Time scale : 1 ms/div.

B. MT applied to the droop loop

The application of the MT to converters implementing droop control, as discussed in Sec. V, is investigated in this subsection. To analyze the stability of the droop loop for each of the converters in Fig. 6, the small-signal perturbation is injected at point B of Fig. 5.

During this test, the three droop-controlled buck converters in Fig. 6 operate in parallel. As discussed in Sec. IV, multiple converters can monitor their stability margins either simultaneously or based on a time division multiplexing algorithm defined by the supervisory controller. Fig. 12 shows the simulation results of the MT applied to the droop loop of the three converters shown in Fig. 6, in both simultaneous and non-simultaneous cases. The expected margins for the droop loop of converter #1 are similar to those of converter #2, which are reported in Table III; differently, the analytically expected stability margins for converter #3 are 195 Hz and 102 deg, for the crossover frequency and phase margin, respectively. As can be seen in Fig. 12, the stability margins monitored on-line in the non-simultaneous case are very close to those expected by the analytical models, reported in Table III. However, in the case of simultaneous perturbations at similar frequencies, the precision slightly decreases, due to the effect of the $\tilde{f}_1 - \tilde{f}_2$ component, as explained while referring to (20). Here, f_{lpf} is set to 1 Hz, which leads to reasonable precision, namely, an error of about 1% for the phase margins and 0.4 % for the crossover frequency, as visible in Fig. 12. Another point worth remarking is that the perturbation coming from converter #3 has negligible effect on the monitored values of the other two converters, thanks to the orthogonality property among sinusoidal signals at different frequencies, as discussed in Sec. IV.B.

As for the experimental results, the monitored stability margins of just one converter (i.e., converter #2) are reported. According to Table III and Fig. 7, on the basis of the transfer function measured by SFRA tool for the droop loop of converter #2, the expected crossover frequency and phase margin are 271 Hz and 90 deg, respectively. The values monitored on-line are 271 Hz and 91 deg, reported in Fig. 13. This close

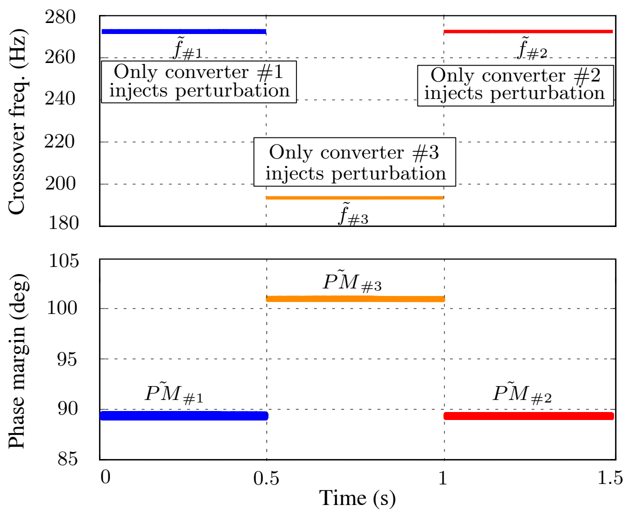

(a) Non-simultaneous monitoring (assigning a monitoring window to each converter)

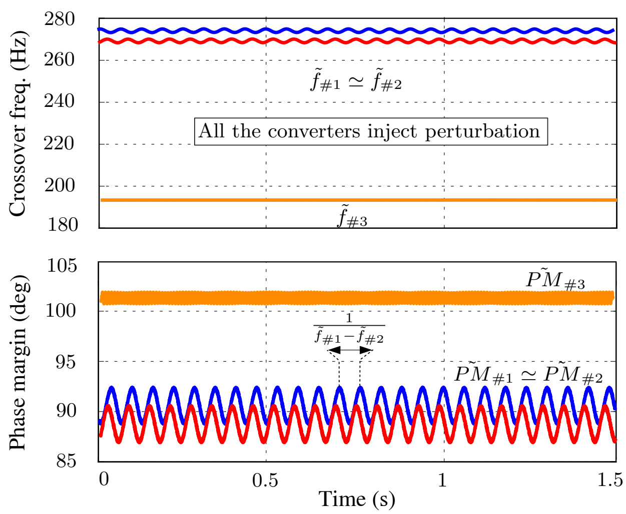

(b) Simultaneous monitoring (decreasing the LPF cut-off frequency)

Fig. 12. MT simulation results considering the droop loop of the converters in Fig. 6. Parameters listed in Table I and Table II.

matching between the estimated and the monitored values proves the effectiveness of the proposed MT applied to the droop control loop. In addition, Fig. 13 shows the ripples in the output voltage and current of the converter that performs the stability monitoring, these ripples measure less than 0.5% of the nominal voltage and 3% of the nominal current. This small effect on the output signals is allowed by choosing the perturbation amplitude $|s_z|$ according to the appendix. By the reported method, values of $|s_z|$ can be identified that are small enough to produce negligible perturbations on the system's operating point but still significantly higher than the noise and the analog-to-digital quantization levels.

As discussed in Sec. III-A, the LPFs used in Fig. 4 have the task to reject the ripple at twice the perturbation frequency. Therefore, their cut-off frequency should be chosen significantly lower than the expected crossover frequency of the loop under investigation. Different attenuation levels, obtained by changing the cut-off frequency or the order of the filter, result

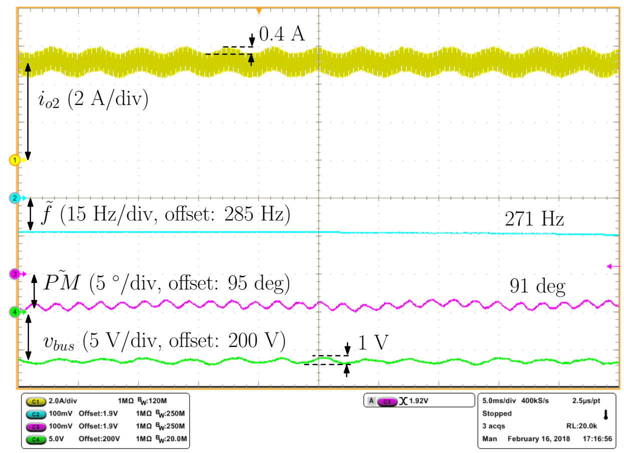

Fig. 13. Experimental results, when the stability monitoring unit is applied to the droop loop of converter #2 in Fig. 6. Output current of converter #2 (i_{o2}), bus voltage (v_{bus}), crossover frequency $\tilde{f}$, and phase margin $\tilde{PM}$. Time scale : 5 ms/div.

in different estimation accuracies. In order to show the effect of different LPF choices on the estimated stability margins, the previous experiment (i.e., droop loop of converter #2) is repeated with three different values of cut-off frequency f_{lpf}. The results are reported in Fig. 14. As can be noticed, the choice of f_{lpf} does not affect the average values of the obtained estimates, but it affects the superimposed sinusoidal fluctuation at $2\tilde{f}$, as highlighted also in (8) and (9). Fig. 14 shows that higher values of f_{lpf}, bring to larger estimation errors—however, the amount of this effect on $\tilde{PM}$ is different from the effect on $\tilde{f}$, due to different signal processing paths: $\tilde{f}$, for example, benefits from the additional filtering action of the integration block $G_{\tilde{f}}$, as described in Fig. 4. In a nutshell, f_{lpf} can be decreased in order to reduce the estimation error, but as addressed in Sec. III-B, it should not be so small to also affect the design of the frequency regulator $G_{\tilde{f}}$.

C. Dynamic behavior of the MT

In previous experiments, the stability monitoring tool was tested in steady-state conditions. In order to further assess the applicability of the proposed MT in dc microgrids, the performance of the method under dynamic conditions is evaluated and reported in this subsection. A transient is applied to the considered microgrid prototype by opening the switch Sw_1 in Fig. 6. The load is initially shared among the three buck converters, but after disconnecting converter #1, the load has to be shared among converters #2 and #3, as shown in Fig. 15. As expected, the droop technique achieves an equal load sharing and bus voltage regulation along the considered test case.

As the transfer functions of the droop loop of converter #2 before and after the transient are different, and the monitored stability margins are expected to show the corresponding changes. After opening the switch Sw_1 in Fig. 6, based on the SFRA results, the phase margin of the droop loop of converter #2 decreases by about 10 deg, while the crossover frequency remains approximately unchanged (i.e., variations $< 3\,\text{Hz}$). This is confirmed by the experimental results displayed in Fig. 16, which reports the experimental results of the MT

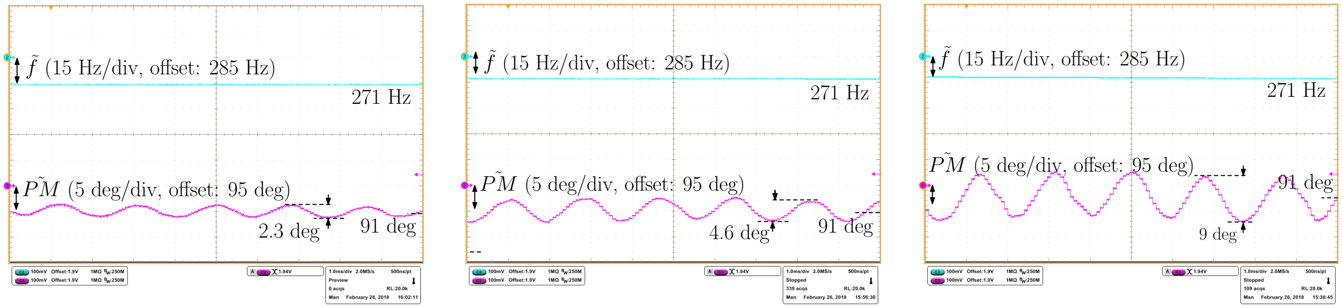

(a) f_{lpf} = 5 Hz (b) f_{lpf} = 10 Hz (c) f_{lpf} = 20 Hz

Fig. 14. The effect of the LPF cut-off frequency on the monitored crossover frequency ($\tilde{f}$) and phase margin ($\tilde{PM}$). Time scale : 1 ms/div.

applied to the droop loop of converter #2, under the the considered transient.

Finally, Fig. 16 also highlights the response time of the MT, which is less than 5 ms, if measured from 10% to 90% of the total variation.

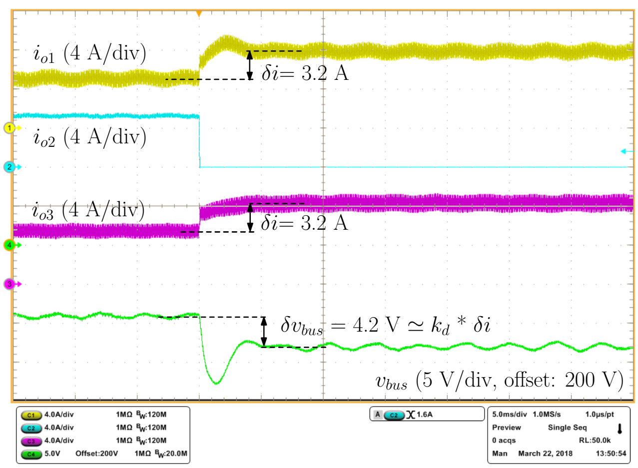

Fig. 15. Performance of the droop control implemented in the converters in Fig. 6. The considered transient: opening the switch Sw_1 in Fig. 6. Time scale : 5 ms/div.

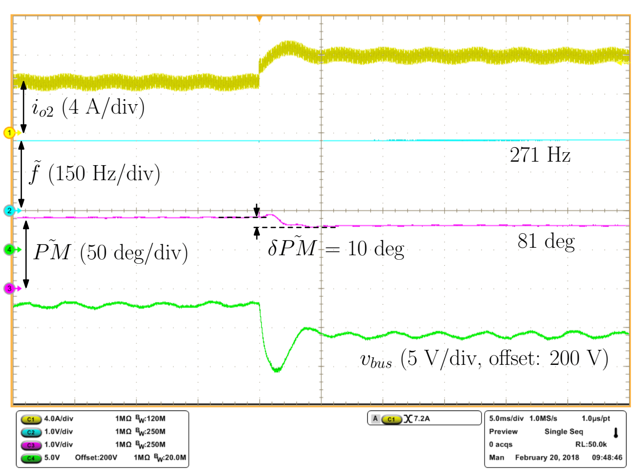

Fig. 16. Performance of the stability monitoring unit applied to the droop loop of converter #2 in Fig. 6, under the transient reported in Fig. 15. Time scale : 5 ms/div.

VII. Conclusion

An on-line stability monitoring technique for power converters operating in dc microgrids is presented in this paper. The technique is inspired by the Middlebrook's injection method, and allows to estimate and monitor the stability margins of any control loop under consideration (e.g., current, voltage, or droop control loops). The proposed monitoring technique is described in details, also discussing the possible design choices and trade-offs. Since the paper targets the application of the method in a multiple-converter environment, which is not specifically addressed in the current literature, the presence of multiple perturbations coming from the monitoring units of several converters is also investigated. In particular a time division multiplexing is considered for the general scenarios, and a small modification is applied in the MT for some particular cases where there is a strict need for simultaneous monitoring of some converters. An experimental setup composed of three buck converters, a constant power load, and a resistive load is implemented to emulate a dc microgrid. The current, the voltage and the droop loops are tested, reporting a close match between the obtained experimental results from the monitoring unit and the values expected from the measured transfer functions. The accuracy obtained in the estimates of the stability margins, in both steady-state and transient conditions, validates the effectiveness of the proposed approach. The reported results also show that the bus voltage and the inductor current are not significantly affected by the small-signal perturbations injected for stability monitoring purposes if the provisions discussed in the paper are applied. In conclusion, the proposed scheme is fast, accurate, and simple, and represents a promising candidate for adaptive control and auto-tuning of power converters within dc microgrids.

Appendix

As mentioned in Sec. III, the choice of the small-signal perturbation amplitude $|s_z|$ does not affect the design of the frequency loop in Fig. 4. However, in order to maintain the effectiveness of the method $|s_z|$ should be chosen appropriately. In particular, the following aspects should be considered:

- Effect of the small-signal perturbation on the output signals. To evaluate this issue, we look at the effect of the perturbation on the bus voltage and the inductor current, because these signals are relevant to the loops considered in this paper. Of course, in the case of having a power loop, the similar consideration can be made for the output power signal. Let us denote the effect of s_z on the bus voltage as s_{zv} and its effect on the inductor current as s_{zi}. Then, in the Laplace domain:

$$s_{zv}(s) = G_{zv}(s)s_z(s), \quad s_{zi}(s) = G_{zi}(s)s_z(s) \quad \text{(A.1)}$$

where $G_{zv}(s)$ is the transfer function from the perturbation signal to the bus voltage and $G_{zi}(s)$ is the transfer function from the perturbation signal to the inductor current. Then:

$$G_{zv}(s) = \frac{v_{bus}(s)}{s_z(s)} = \frac{v_{bus}(s)}{s_x(s)}.\frac{s_x(s)}{s_z(s)} = \frac{G_{xv}(s)}{1+T(s)} \quad \text{(A.2)}$$

where $T(s)$ is the open loop transfer function of the considered loop and $G_{xv}(s)$ is the transfer function from the perturbation point to the bus voltage, which can be analytically derived. The same process can be used to find $G_{zi}(s)$, too.

For any system under study, $|s_z|$ must be large enough to obtain:

$$|G_{zv}(\tilde{f})|.|s_z| \gg s_{nv}, \quad |G_{zi}(\tilde{f})|.|s_z| \gg s_{ni} \quad \text{(A.3)}$$

where s_{nv} and s_{ni} are the noise levels on the bus voltage and on the inductor current, respectively. In this way, the minimum value of the perturbation amplitude is determined. For what concerns the maximum value, $|s_z|$ should be small enough to be considered as a small-signal value, so that the perturbation signal does not deteriorate the output signals.

- Effect of the small-signal perturbation on the dynamics of the frequency loop. The steady-state result of the frequency estimator does not depend on $|s_z|$, but its dynamics does [as shown in (14), (15), (16)].

References

[1] P. Wang, L. Goel, X. Liu, and F. H. Choo, "Harmonizing ac and dc: A hybrid ac/dc future grid solution," *IEEE Power and Energy Magazine*, vol. 11, no. 3, pp. 76–83, 2013.

[2] L. Meng, A. Luna, E. R. Díaz, B. Sun, T. Dragicevic, M. Savaghebi, J. C. Vasquez, J. M. Guerrero, M. Graells, and F. Andrade, "Flexible system integration and advanced hierarchical control architectures in the microgrid research laboratory of aalborg university," *IEEE Transactions on Industry Applications*, vol. 52, no. 2, pp. 1736–1749, 2016.

[3] Y. Gu, W. Li, and X. He, "Frequency-coordinating virtual impedance for autonomous power management of dc microgrid," *IEEE Transactions on Power Electronics*, vol. 30, no. 4, pp. 2328–2337, April 2015.

[4] X. Lu, J. M. Guerrero, K. Sun, and J. C. Vasquez, "An improved droop control method for dc microgrids based on low bandwidth communication with dc bus voltage restoration and enhanced current sharing accuracy," *IEEE Transactions on Power Electronics*, vol. 29, no. 4, pp. 1800–1812, April 2014.

[5] G. Venkataramanan and C. Marnay, "A larger role for microgrids," *IEEE Power and Energy Magazine*, vol. 6, no. 3, pp. 78–82, May 2008.

[6] T. Dragicevic, J. C. Vasquez, J. M. Guerrero, and D. Skrlec, "Advanced lvdc electrical power architectures and microgrids: A step toward a new generation of power distribution networks." *IEEE Electrification Magazine*, vol. 2, no. 1, pp. 54–65, March 2014.

[7] X. Feng, J. Liu, and F. C. Lee, "Impedance specifications for stable dc distributed power systems," *IEEE Transactions on Power Electronics*, vol. 17, no. 2, pp. 157 – 162, March 2002.

[8] R. D. Middlebrook, "Input filter considerations in design and application of switching regulators," *IEEE Industry Applications Society Annual Meeting, Chicago. Oct,1976*, pp. 366–382.

[9] A. Riccobono, M. Cupelli, A. Monti, E. Santi, T. Roinila, H. Abdollahi, S. Arrua, and R. A. Dougal, "Stability of shipboard dc power distribution: Online impedance-based systems methods," *IEEE Electrification Magazine*, vol. 5, no. 3, pp. 55–67, 2017.

[10] E. Santi, H. Y. Cho, A. B. Barkley, D. Martin, and A. Riccobono, "Tools to address system level issues in power electronics: The digital network analyzer method and the positive feedforward control technique," in *IEEE 8th International Conference on Power Electronics and ECCE Asia (ICPE & ECCE), 2011*, pp. 2106–2113.

[11] B. Miao, R. Zane, and D. Maksimovic, "Practical on-line identification of power converter dynamic responses," in *IEEE Twentieth Annual Applied Power Electronics Conference and Exposition (APEC 2005)*, pp. 57–62.

[12] W. Stefanutti, P. Mattavelli, S. Saggini, and M. Ghioni, "Autotuning of digitally controlled dc–dc converters based on relay feedback," *IEEE Transactions on Power Electronics*, vol. 22, no. 1, pp. 199–207, 2007.

[13] I. Kaya and D. P. Atherton, "Exact parameter estimation from relay autotuning under static load disturbances," in *Proceedings of the American Control Conference,2001*, pp. 3274–3279.

[14] J. Liu, X. Feng, F. C. Lee, and D. Borojevich, "Stability margin monitoring for dc distributed power systems via perturbation approaches," *IEEE transactions on power electronics*, vol. 18, no. 6, pp. 1254–1261, 2003.

[15] A. Barkley and E. Santi, "Improved online identification of a dc–dc converter and its control loop gain using cross-correlation methods," *IEEE Transactions on power electronics*, vol. 24, no. 8, pp. 2021–2031, 2009.

[16] T. Roinila, M. Vilkko, and T. Suntio, "Fast loop gain measurement of a switched-mode converter using a binary signal with a specified fourier amplitude spectrum," *IEEE Transactions on Power Electronics*, vol. 24, no. 12, pp. 2746–2755, 2009.

[17] M. Bhardwaj, S. Choudhury, R. Poley, and B. Akin, "Online frequency response analysis: A powerful plug-in tool for compensation design and health assessment of digitally controlled power converters," *IEEE Transactions on Industry Applications*, vol. 52, no. 3, pp. 2426–2435, 2016.

[18] G. E. Pitel and P. T. Krein, "Real-time system identification for load monitoring and transient handling of dc-dc supplies," in *IEEE Power Electronics Specialists Conference (PESC 2008)*, pp. 3807–3813.

[19] M. M. F. S. Algreer, "Microprocessor based signal processing techniques for system identification and adaptive control of dc-dc converters," Ph.D. dissertation, School of Electrical and Electronic Engineering, Newcastle University, UK, 2012.

[20] R. D. Middlebrook, "Measurement of loop gain in feedback systems," *International Journal of Electronics Theoretical and Experimental*, vol. 38, no. 4, pp. 485–512, 1975.

[21] J. Morroni, R. Zane, and D. Maksimovic, "An online stability margin monitor for digitally controlled switched-mode power supplies," *IEEE Transactions on Power Electronics*, vol. 24, no. 11, pp. 2639–2648, 2009.

[22] A. Khodamoradi, G. Liu, P. Mattavelli, T. Caldognetto, and P. Magnone, "On-line stability monitoring for power converters in dc microgrids," in *2017 IEEE Second International Conference on DC Microgrids (ICDCM)*, pp. 302–308.

[23] T. Strasser, F. Andrén, J. Kathan, C. Cecati, C. Buccella, P. Siano, P. Leitão, G. Zhabelova, V. Vyatkin, P. Vrba, and V. Mařík, "A Review of Architectures and Concepts for Intelligence in Future Electric Energy Systems," *IEEE Transactions on Industrial Electronics*, vol. 62, no. 4, pp. 2424–2438, April 2015.

[24] L. Corradini, D. Maksimović, P. Mattavelli, and R. Zane, *Digital control of high-frequency switched-mode power converters*. John Wiley & Sons, 2015, vol. 48.

[25] T. Roinila, T. Messo, and E. Santi, "Mimo-identification techniques for rapid impedance-based stability assessment of three phase systems in dq domain," *IEEE Transactions on Power Electronics, Issue. 99*, 2017.

[26] T. Roinila, H. Abdollahi, S. Arrua, and E. Santi, "Online measurement of bus impedance of interconnected power electronics systems: Applying orthogonal sequences," in *2017 IEEE Energy Conversion Congress and Exposition (ECCE)*, pp. 5783–5788.

[27] J. G. Proakis, M. Salehi, N. Zhou, and X. Li, *Communication systems engineering*. Prentice Hall New Jersey, 1994, vol. 2.

[28] P. Tenti, A. Costabeber, P. Mattavelli, and D. Trombetti, "Distribution loss minimization by token ring control of power electronic interfaces in residential microgrids," *IEEE Transactions on Industrial Electronics*, vol. 59, no. 10, pp. 3817–3826, 2012.

[29] S. I. Gkavanoudis, K. O. Oureilidis, and C. S. Demoulias, "An adaptive droop control method for balancing the soc of distributed batteries in

ac microgrids," in *IEEE 17th Workshop on Control and Modeling for Power Electronics (COMPEL), 2016*, pp. 1–6.
[30] "SFRA tool." [Online]. Available: http://www.ti.com/tool/SFRA

Aram Khodamoradi (S'17) received the B.S. and M.S. degrees in electrical engineering from Shahid Beheshti University (Iran), and University of Siena (Italy), respectively in 2013, and 2016. He is currently working towards Ph.D. degree at the University of Padova (Italy).

His research interests include stability monitoring and auto-tuning of dc microgrids power converters, and impedance-based stability analysis.

Guangyuan Liu (S'17) received the B.E. degree in electrical engineering and automation from Tsinghua University (China) in 2013 and the M.S. degree in electrical engineering from Zhejiang University (China) in 2016. He is currently working towards Ph.D. degree in the University of Padova (Italy).

His research interests include modeling and control of power electronic converters, particularly for distributed energy resources in dc microgrids.

Paolo Mattavelli (S'95, A'96, M'00, SM'10, F'14) received the MS degree (with honors) and the Ph. D. degree in electrical engineering from the University of Padova (Italy) in 1992 and in 1995, respectively. From 1995 to 2001, he was a researcher at the University of Padova. From 2001 to 2005 he was an associate professor the University of Udine, where he led the Power Electronics Laboratory. In 2005 he joined the University of Padova in Vicenza with the same duties. From 2010 to 2012 he was professor and member of the Center for Power Electronics Systems (CPES) at Virginia Tech. He is currently a professor with the University of Padova.

His major field of interest includes analysis, modeling and analog and digital control of power converters, grid-connected converters for renewable energy systems and micro-grids, high-temperature and high-power density power electronics. In these research fields, he has been leading several industrial and government projects. His current google scholar h-index is 64.

From 2003 to 2012 he served as an Associate Editor for IEEE Transactions on Power Electronics. From 2005 to 2010 he was the IPCC (Industrial Power Converter Committee) Technical Review Chair for the IEEE Transactions on Industry Applications. For terms 2003-2006, 2006-2009 and 2013-2015 he has been a member-at-large of the IEEE Power Electronics Societys Administrative Committee. He also received in 2005, 2006, 2011 and 2012 the Prize Paper Award in the IEEE Transactions on Power Electronics and in 2007, the 2nd Prize Paper Award at the IEEE Industry Application Annual Meeting. He is an IEEE Fellow.

Tommaso Caldognetto (S'10, M'16) received the M.S. (Hons.) degree in electronic engineering and the Ph.D. degree in information engineering from the University of Padova, Italy, in 2012 and 2016, respectively.

In 2014, he was a visiting Ph.D. student with the Institute for Automation of Complex Power Systems, University of Aachen, Germany. He is currently a researcher with the Department of Technology and Management, University of Padova. His research interests include control of grid-tied converters, microgrid architectures, and real-time simulation for power electronics.

Paolo Magnone received the B.S. and M.S. degrees in electronic engineering from the University of Calabria, Rende, Italy, in 2003 and 2005, respectively, and the Ph.D. degree in electronic engineering from the University of Reggio Calabria, Italy, in 2009.

In the period 2006-2008 he joined for one year the Interuniversity MicroElectronics Center (IMEC), Leuven, Belgium, within the Advanced PROcess Technologies for Horizontal Integration project (Marie Curie Actions), where he worked on parameters extraction and matching analysis of FinFET devices. From 2009 to 2010, he was a Postdoctoral Researcher with the University of Calabria. From 2010 to 2014, he was with the Advanced Research Center on Electronic Systems for Information and Communication Technologies E. De Castro (ARCES), University of Bologna, Italy. In 2014, he was appointed Associate Professor of electronics at the University of Padova, Italy. His current research interests include the electrical characterization and modeling of semiconductor devices and circuits for power applications.